

Original Article

Analysis of ligustrazine covalent cyclodextrin frameworks in bioinformatics and network pharmacology-based acute lung injury treatment

Di Wu^{a,b,c}, Xiao Le Wang^d, Yu Jia^b, Si Yu He^e, Ya Ting Gao^{a,b,c}, Qin Jun Yang^{b,c}, Huan Zhang Ding^{a,b,c}, Tong Liu^b, Meng Yao Shi^b, Ji Wen Zhang^e, Jie Zhu^{b,*}, Ze Geng Li^{a,b,c,*}

^aThe First Affiliated Hospital of Anhui University of Chinese Medicine, Hefei, China

^bAnhui University of Chinese Medicine, Hefei, China

^cAnhui Province Key Laboratory of the Application and Transformation of Traditional Chinese Medicine in the Prevention and Treatment of Major Pulmonary Diseases, Hefei, China

^dAffiliated Hospital of Jiangxi University of Chinese Medicine, Nanchang, China

^eCenter for Drug Delivery Systems, Shanghai Institute of Materia Medica, Chinese Academy of Sciences, Shanghai, China

ARTICLE INFO

Keywords:

Acute lung injury
Bioinformatics
Covalent cyclodextrin frameworks
Ligustrazine
Pulmonary drug delivery

ABSTRACT

Acute lung injury (ALI) is a grave and potentially fatal acute inflammatory condition. Ligustrazine (LIG), an active ingredient in traditional Chinese medicine (TCM), has been proven to inhibit ALI oxidative stress and inflammatory responses; however, its mechanism of ALI treatment remains unclear. We investigated the molecular mechanism of LIG covalent cyclodextrin backbone (LIG-OC-COF) granules in ALI treatment. Network pharmacology identified 16 potential LIG targets, including *BCL2L1*, *JAK2*, *CDK2*, *HIF1A*, and *CCNA2*. The Kyoto encyclopedia of genes and genomes (KEGG) pathway analysis suggested that these points were involved in the Janus kinase/signal transducer and activator of transcription (JAK/STATs) signaling pathway. The results from the molecular docking further confirmed the stable binding affinity between target proteins and LIG. *In vivo* experiments revealed that LIG downregulated the expression of pro-inflammatory factors (i.e., Tumor Necrosis Factor- α (TNF- α), Interleukin - 1 β (IL-1 β), and Interleukin - 6 (IL-6); $P < 0.0001$) and upregulated the expression of the anti-inflammatory factor (i.e., IL-10; $P < 0.0001$) in the serum of ALI rat models. This effectively alleviated the apoptosis of ALI lung cells ($P < 0.0001$) and downregulated the mRNA expression of the aforementioned key targets ($P < 0.0001$) and the related proteins in the JAK2/STAT3 signaling pathway ($P < 0.0001$). The inhalation of LIG-covalent cyclodextrin frameworks (LIG-OC-COF) may exert its therapeutic effect by modulating the expression of key target molecules. LIG exhibits an anti-inflammatory and anti-apoptotic effect on lung tissues by regulating the *BCL2L1*, *JAK2*, *CDK2*, *HIF1A*, and *CCNA2* molecules and affecting the activation of the JAK/STAT signaling pathway. LIG-OC-COF can enhance these changes. LIG-OC-COF granules targeting lung delivery of LIG is an effective ALI treatment.

1. Introduction

Acute lung injury (ALI) is identified as an initial inflammatory disease of the pulmonary system [1] that can easily progress to acute respiratory distress syndrome (ARDS), boasting a 40% fatality rate. [2]. ALI involves alveolar structure damage, tissue barrier destruction, and accumulation of numerous inflammatory cells [3,4]. Although ALI has been extensively studied for decades, effective drug-based treatment strategies are lacking. Growing evidence suggests that natural active ingredients of traditional Chinese medicine (TCM) can interfere with disease progression in multiple ways. For example, ligustrazine (LIG) can effectively decrease inflammatory cell aggregation, alleviate inflammatory damage in lung tissues [5,6], and reduce clinical symptoms of ALI.

LIG is an alkaloid isolated and purified from the TCM *Ligusticum chuanxiong hort* (Chuan Xiong). This natural substance has a number of pharmacological properties, including anti-inflammatory, antioxidant [7], and anti-apoptotic properties [8]. However, orally administered

LIG has some limitations, such as a first-pass effect, relatively shorter biological half-life, and poor bioavailability [9]. Therefore, frequent long-term dosing is required to maintain effective blood concentration, which may easily cause drug accumulation in the body and increase the related toxicity and side effects. As a result, improving LIG bioavailability and exploring new dosage forms and administration routes have become hot research topics.

The pulmonary targeted drug delivery system presents the benefits of a large absorption surface area, rich blood flow, thin epithelial barrier, and high permeability, which makes it an ideal drug delivery route for pulmonary disease treatments [10]. Drugs and biomolecules can be loaded into the multipurpose crystalline substance known as the cyclodextrin metal-organic framework (CD-MOF). Its pore structure, thermal stability, biocompatibility, and specific surface area are all outstanding [11,12]. Several studies have indicated that CD-MOFs exhibit significant efficacy when loaded with drugs such as ibuprofen, captopril, and lansoprazole [13-15]. Our past study [16] demonstrated that, when paeonol (PAE) is loaded into the CD-MOF, the prepared

*Corresponding authors:

E-mail addresses: janezhutcm@foxmail.com (J. Zhu), ahzyfb@sina.com (Z. Li)

Received: 03 December, 2024 Accepted: 19 March, 2025 Epub Ahead of Print: 15 May 2025 Published: 21 May 2025

DOI: 10.25259/AJC_219_2024

PAE-CD-MOF can significantly improve bioavailability, achieve efficient delivery of lung therapy drugs, and reduce the inflammation of the lung tissues. Further, our research could enhance the mobility and atomization of CD-MOFs. [17]. We synthesized a novel kind of biodegradable and reactive oxygen species (ROS)-sensitive cross-linked covalent cyclodextrin frameworks (OC-COF). In this process, CD-MOF, which contains abundant hydroxyl groups, was utilized for modification. In addition, oxalyl chloride (OC) was chosen as an H_2O_2 -labile precursor to introduce peroxalate ester bonds into OC-COF. This step helped hydrolyze and clear the ROS produced at the inflammatory sites, thereby improving the therapeutic effect. Past studies [18] have confirmed that the dry-powder inhaler (DPI) LIG-OC-COF prepared by loading LIG into the OC-COF is safe and reliable, with good aerodynamic properties and a significant anti-inflammatory effect, thereby regulating inflammatory reaction and oxidative stress in the lungs of ALI-affected rats. Nevertheless, its action mechanism remains unclear.

Therefore, we employed network pharmacology and bioinformatics methods to analyze the potential targets and pathways of LIG for ALI treatment. We also verified oral and inhaled preparations using *in vivo* experiments to investigate the possible mechanism of altering the LIG delivery form to improve ALI efficacy (Figure 1).

2. Materials & Methods

2.1. Network pharmacology data preparation

2.1.1. Potential target prediction of LIG in ALI treatment

The Traditional Chinese Medicine Systems Pharmacology Database and Analysis Platform (TCMSP) (<http://tcmsp.com/>), PharmMapper (<http://www.lilab-ecust.cn/pharmmapper>), and SwissTargetPrediction database (<http://swisstargetprediction.ch/>) were searched to find the target LIG genes. The LIG targets were obtained from the TCMSP database using the term “ligustrazine”. Then, the *.mol2 file of LIG was downloaded, and the *.mol2 file was uploaded to the PharmMapper website. All targets (v2010, 7302) were selected, and the other parameters retained their default settings. The SwissTargetPrediction

database (<http://swisstargetprediction.ch/>) was accessed by entering the Simplified Molecular Input Line Entry System (SMILES) number of LIG that was obtained from the PubChem database (<https://pubchem.ncbi.nlm.nih.gov/>). The “Homo sapiens” was selected to obtain the target of LIG.

2.1.2. Differentially expressed genes of ALI

2.1.2.1. Chip data source

The ALI-related gene profiles were obtained from the public online database—Gene Expression Database (<https://www.ncbi.nlm.nih.gov/>), and the required data was obtained after filtering.

2.1.2.2. Inclusion criteria

By setting the search formula ((Lipopolysaccharide OR LPS) AND (acute lung injury OR ALI)), a search was performed in the Gene expression omnibus (GEO) database. The inclusion criteria for screening the dataset were also set: (1) the study contained individual data from both normal controls and ALI of all species with a sample size of ≥ 3 each; (2) the intervention factor of the study: LPS; (3) the detection samples were collected: bronchoalveolar lavage fluid, lung tissue, and serum; (4) the study contained available raw data with available gene annotation files.

To ensure that differential genes were significantly expressed in all species, two gene microarray data files were obtained after screening, including GSE111241 (Rat) and GSE2411 (Mouse); however, no data on humans were found. Therefore, 9 samples each from the LPS and normal groups were included. The details of the dataset have been shown in Table 1.

The difference analysis was performed by utilizing the Limma package in the R language [19]. $P < 0.05$ was considered to indicate differentially expressed genes (DEGs), and Benjamini—Hochberg was adopted to adjust the P -values in DEG analysis, while ggplot2 package and ggthemes were used to draw volcano maps of DEGs. These DEGs were then used for the mapping of the LIG target genes.

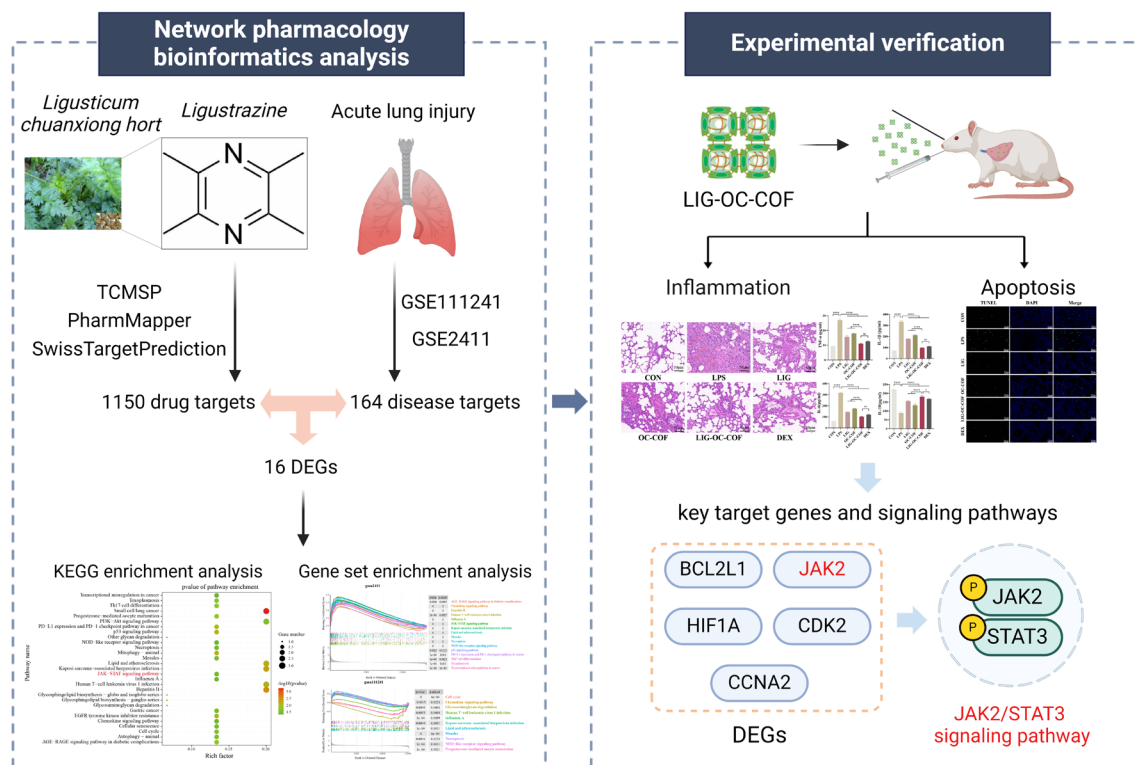


Figure 1. The workflow depicting the study design.

Table 1. Features of the selected dataset series.

GSE number	Organisms	Number of ALI samples	Number of normal samples	Sample type	Platforms
GSE111241	Rat	3	3	Bronchoalveolar lavage fluid	GPL1355 [Rat230_2] Affymetrix Rat Genome 230 2.0 Array
GSE2411	Mouse	6	6	lung tissue	GPL339 [MOE430A] Affymetrix Mouse Expression 430A Array

2.1.3. Target prediction and hub gene identification of LIG in ALI treatment

The R language (R version 3.6.3) was used to map the obtained LIG targets to the differentially expressed ALI genes, and the R package was used to establish the target gene network of LIG for ALI treatment. To understand the interaction relationship between these successfully mapped differential genes and the hub genes in them, we performed the protein-protein interaction (PPI) analysis on these differential genes by using the STRING web tool, and Cytoscape software was used to draw the PPI network diagrams. Meanwhile, 12 algorithms of the cytoHubba plugin of the software were used to analyze the hub genes of the network. The top 10 hub genes of each algorithm were screened, and Sankey diagram of the hub genes was visualized with the aid of the networkD3 package.

2.1.4. Kyoto Encyclopedia of Genes and Genomes (KEGG) enrichment analysis of DEGs in LIG-treated ALI

To comprehend the molecular mechanisms underlying LIG-mediated ALI treatment, the KEGG enrichment analysis was performed on successfully mapped differential genes. The differential genes associated with LIG-treated ALI were imported into R software, and the R package clusterProfiler [20] was used to conduct the KEGG pathway enrichment analysis, after which the bubble chart of the significantly enriched top 30 pathways was drawn.

2.1.5. Gene set enrichment analysis based on ALI genes

Although we identified the possible molecular biological pathways related to the differential genes associated with LIG-treated ALI, these pathways may not have crucial significance in ALI pathogenesis. Therefore, utilizing the outcomes from the ALI differential analysis, the R package clusterProfiler was utilized to perform gene set enrichment analysis (GSEA), especially the significant enrichment.

2.1.6. Molecular docking verification

The Pubchem database (<https://pubchem.ncbi.nlm.nih.gov/>) provided the structure for LIG. B-cell lymphoma 2-like protein 1 (BCL2L1), Janus kinase 2 (JAK2), Hypoxia-inducible factor 1 α (HIF1A), Cyclin-dependent kinase 2 (CDK2) and Cell cycle protein A2 (CCNA2) crystal structures were retrieved from the PDB database (<https://www.rcsb.org/>). Pymol-2.1.0 software was used to improve the target proteins by removing small molecule ligands and water molecules. Then, the proteins were also performed for hydrogenation and calculated charge with AutoDock Tools-1.5.6 and saved as pdbqt format. Energy minimization of LIG was performed using the PyRx built-in tool (OpenBabel). The molecular docking of the proteins with LIG was accomplished through the vina-2.0 module within PyRx software, entailing the calculation of binding energy and the generation of output files. Finally, the Discovery Studio 2020 Client (<https://discover.3ds.com/discovery-studio-visualizer-download>) was used for visualization. The binding strength between the two was represented by the affinity value (kcal/mol); the decrease in binding energy was concomitant with an enhancement in the stability of the ligand-receptor binding.

2.2. Experimental verification

2.2.1. Materials

MaxDragon Biochem Ltd. (Guangdong, China) provided the γ -CD. McLean Biochemistry Technology Co., Ltd. (Shanghai, China) supplied LIG. Dichloromethane (DCM) was supplied by Bellingway Technology Co., Ltd. (Shanghai, China). Sigma (USA) supplied the lipopolysaccharide (LPS) (L2880). The Shanghai Institute of Materia Medica, Chinese Academy of Sciences (Shanghai, China), provided the LIG-OC-COF and OC-COF. China's Beijing Solarbio Technology Co., Ltd. is the supplier of dexamethasone (DEX; D8040). The primers for quantitative real-time polymerase chain reaction (qRT-PCR) were fabricated in Servicebio Technology Co., Ltd. (Wuhan, China). Antibodies included JAK1 (YT2424), phospho-JAK1 (pJAK1) (Tyr1022) (YP0154), phospho-JAK2 (pJAK2) (Tyr1007) (YP0155), JAK3 (YT2430), pJAK3 (Tyr785) (YP0756), and GAPDH (YN3029) were all obtained from ImmunoWay Biotechnology (USA), JAK2 (bs-0908R) and Phospho-signal transducer and activator of transcription 3 (pSTAT3) (Tyr705) (bs-1658R) from Bioss (Beijing, China), and Signal transducer and activator of transcription 3 (STAT3) (60199-1-Ig) from Proteintech (Wuhan, China). Rat tumor necrosis factor- α (TNF- α) (EK382/3-48), Interleukin - 1 β (IL-1 β) (EK301B/3-48), Interleukin - 6 (IL-6) (EK310/2-48), and Interleukin - 10 (IL-10) (EK310/2-48) enzyme-linked immunosorbent assay (ELISA) kits were purchased from Multisciences (Hangzhou, China).

2.2.2. Synthesis of OC-COF

The synthesis of the CD-MOF and OC-MOF was done following our previously reported method [13] (Liu *et al.*, 2016). Cuboidal CD-MOF particles were first prepared by dissolving γ -CD (14.584 g) and KOH (5.049 g) in deionized water (450 mL, 18.2 M Ω -cm), followed by filtration and mixing with methanol (60 mL) in a closed system. The solution was heated at 60°C, supplemented with Polyethylene glycol (PEG) 20000 (640 mg) as a size regulator, and cooled in a cold-water bath for 2–3 hrs. The deposition was washed twice with methanol and ethanol to remove impurities and dried in a vacuum at 80°C, and CD-MOF was obtained. Subsequently, 3 g of CD-MOF was weighed into a flask and mixed with 30 mL of dehydrated DCM. At 4°C, TEA (1 mL) was added as a catalyst, and OC (2181 μ L) was added dropwise into anhydrous DCM (10 mL). The resulting mixture was kept in nitrogen at room temperature for 24 hrs. The product was centrifuged, sequentially washed with anhydrous ether, ethanol, 50% ethanol, and water to remove residues, and finally freeze-dried to obtain OC-COF.

2.2.3. Preparation of LIG-OC-COF

Anhydrous ethanol (5 mL) was used to completely dissolve LIG (4 g), to which OC-COF (1 g) was added. The solution was centrifuged, and the supernatant was discarded. Finally, the mixture (LIG-OC-COF) was subjected to further characterization. Eq. (1) was utilized to ascertain the amount of drug loading. The detailed preparation processes of LIG-OC-COF, hydrolysis property, cytotoxicity evaluation, transepithelial transport studies, and pharmacokinetic studies have been provided in our past paper [18].

$$\text{Drug loading amount of LIG (\%)} = \frac{M_{\text{drug loaded in LIG-OC-COF}}}{M_{\text{LIG-OC-COF}}} \times 100\% \quad (1)$$

2.2.4. Animal experiments

Male Sprague-Dawley rats weighing 200–220 g and aged 6–8 weeks were acquired from Hangzhou Medical College's Animal Experiment Center [experimental animal production license number: SCXK (Zhe) 2019-0002]. Every experimental protocol complied with the guidelines set forth by the Anhui University of Chinese Medicine's Experimental Animal Ethics Committee (No. AHUCM-rats-2021021).

2.2.5. LPS-induced ALI rat models

Following the acclimatization period, all rats were divided into 6 groups of 8 at random: control group (CON), LPS group (LPS), LPS+LIG-

OC-COF group (LIG-OC-COF), LPS + blank vehicle group (OC-COF), LPS+LIG gavage group (LIG), and LPS + dexamethasone group (DEX). According to our previous modeling method [16,18], the ALI rat model was established with LPS. With the exception of the control group, the rats in the remaining groups were then anesthetized via 2% isoflurane inhalation and fixed in a supine position on a homemade rat board, the airway entrance was exposed, and LPS (8 mg/kg) was injected rapidly into the lungs from the trachea using a micro-sprayer (Penn-Century, Philadelphia, PA, USA); the rats were kept upright and gently shaken from side to side for 10 seconds to diffuse the LPS evenly. An identical volume of regular saline was injected into the control group. After 2 hrs of LPS intervention, the rats received intragastric administration of LIG, whereas OC-COF, LIG-OC-COF, and DEX were inhaled using a dry insufflator (DP-4R, Penn Century). DEX was used as a positive control, and administered a dose of 3 mg/kg. Since the intragastric dose for the LIG group was 42 mg/kg, which is equivalent to the clinical dose, the inhalation dose of LIG was determined to be 8.4 mg/kg, or one-fifth of the gavage dose. Consequently, based on the drug loading content, the dosage of OC-COF was 25.64 mg/kg, whereas the dosage of LIG-OC-COF was found to be 34.04 mg/kg. For the control and model groups, regular saline was utilized. Blood samples were collected from the abdominal aortae following a 6-h treatment period. The left upper lobe of the lung was stabilized using a 4% paraformaldehyde solution. The remaining lung lobe was individually stored in cryopreservation tubes at -80°C. Animal carcasses were sealed in medical waste bags and transported to the Experimental Animal Center of Anhui University of Chinese Medicine for centralized incineration in accordance with bioethical disposal protocols.

2.2.6. Lung histopathological examination

Following the steps of dehydration, embedding, sectioning, rehydration, staining, differentiation, bluing, dehydration, and mounting, the histopathological abnormalities in lung tissue were examined under a light microscope (Leica, DM11, Germany). With reference to a previously reported method [21], alveolar congestion, bleeding, and inflammatory cell infiltration were examined. Subjective quantitative analysis was performed by grading on a scale of 0–4 points: 0 = no lesions or very mild lesions, 1 = mild lesions, 2 = moderate lesions, 3 = severe lesions, and 4 = very severe lesions.

2.2.7. Detection of serum inflammatory factors

According to the experimental design, the standard hole set, CON, LPS, LIG-OC-COF, OC-COF, LPS+LIG LIG, and DEX, were set up. The standard well group received 100 µL of the standard material, whereas the other sample wells received proportionate additions of the matching serum and detection buffer, including TNF-α (1:9), IL-1β (1:4), IL-6 (1:4), and IL-10 (1:4), for a total of 100 µL/well. Then, 50 µL of antibody (1:100 diluted) was immediately added to each well. After incubation and washing, each well was treated with 100 µL of diluted streptavidin-HRP and incubated again for 45 mins. The plate was treated with 100 µL of the standard hole color development substrate TMB. Finally, the microplate spectrophotometer (BioTek EPOCH2) was used to measure the optical density value (OD) at 450 nm [22,23].

2.2.8. TdT-mediated dUTP nick-end labeling (TUNEL) assay

The following dual-staining method was utilized (Servicebio, G1501): apoptotic nuclei were quantified using TUNEL labeling (green fluorescence), while the total number of nuclei was ascertained using 4',6-diamidino-2-phenylindole (DAPI) staining (blue fluorescence) (Servicebio, G1401). A fluorescence microscope (Ortho-Fluorescent Microscopy, NIKON ECLIPSE C1, Japan) was used to view the stained samples at emission wavelengths of 420 and 530 nm. After selecting five non-overlapping fields of view for each sample, Image-Pro Plus software was used to determine the apoptotic index (%) as follows: TUNEL-positive cells divided by total cells times 100% is the apoptotic index (%).

2.2.9. Differential mRNA expression levels in the lung tissues

The extraction of total RNA from lung tissue (ES Science, RN001, China). The concentration and purity of the RNA were assessed using

Table 2. Primers used in the present qRT-PCR study.

Gene	Primer sequences (5'-3')	GenBank accession no.	Product size (bp)
BCL2L1	GTGCGTGAAAAGCGTAGACAA(F)	NM_001033670.1	242
	TGAAGAGTGAGCCCAGCAGAAC(R)		
JAK2	CAGCAAATAAAGAAGGCAGGA(F)	NM_031514.1	103
	TTCTCGTCAACGGCAAAG(R)		
CDK2	AGTTGACGGGAGAAGTTGTGGC(F)	NM_199501.1	126
	GCTTGACGATGTTAGGGTGATG(R)		
HIF1A	ACCGTGCCCTACTATGTGCG(F)	NM_024359.1	197
	GCCTTGTATGGGAGCATTAAC(T)		
CCNA2	CCTTCTATAAACGATGAGCAGC(F)	NM_053702.3	239
	CATGGGGTGATTCAAACACTACC(R)		
GAPDH	CTGGAGAAACCTGCCAAGTATG(F)	NM_017008.4	138
	GGTGAAGAATGGGAGTGTCT(R)		

the NanoDrop 2000 Ultrafine Spectrophotometer. The entire RNA was reverse-transcribed into cDNA using the First-Strand cDNA Synthesis Kit (Servicebio, Catalog No. G3330). qRT-PCR was carried out using a 2× synergy brands (SYBR) Green qPCR Master Mix (None ROX) using reverse transcription-polymerase chain reaction (RT-PCR) equipment (Servicebio, G3320). Three independent samples were used for each experiment. The reaction conditions were as instructed. The relative quantitative analysis was calculated by the 2^{-ΔΔCt} method. The primer sequences have been presented in Table 2.

2.2.10. Related protein expression levels determined via western blotting

Radio immunoprecipitation assay (RIPA) lysis buffer (1% PMSF and 1% proteinase inhibitor) was used to extract the total proteins from each lung tissue. Equal amounts of protein samples were separated using 10% sodium dodecyl sulfate polyacrylamide gel electrophoresis (SDS-PAGE) gel electrophoresis and then transferred to a polyvinylidene fluoride (PVDF) membrane. The membranes were blocked with 5% bovine serum albumin (BSA) for 1 hr, and then they were incubated with primary antibodies at 4°C for the entire night. The membranes were then treated with the corresponding secondary antibodies coupled with horseradish peroxidase for 1 hr at room temperature. The UVP ChemiStudio815 imaging system was used to visualize the protein bands after they were detected using an enhanced chemiluminescence kit. The grayscale analysis of proteins was conducted using ImageJ 2.1.0 software.

2.2.11. Immunohistochemical detection of JAK2/STAT3 signaling pathway proteins in the lung tissues

The paraffin sections of lung tissue from each group of rats were subjected to routine dewaxing, microwave repair, rinsing, and blocking, followed by the removal of the BSA solution. Then, approximately 50 µL of diluted primary antibodies JAK2 (1:300), pJAK2 (1:300), STAT3 (1:500), and pSTAT3 (1:300) were added to each section, and kept at 4°C for the entire night. At room temperature, the secondary antibody was incubated. This step was followed by treatment with diaminobenzidine (DAB) for color development (Servicebio, G1211), hematoxylin restaining, hydrochloric acid–alcohol differentiation, gradient alcohol dehydration, xylene clearing, air drying, and neutral resin sealing. Each group included 3 samples, and 4 visual fields were randomly selected for detection. Image-Pro-Plus analysis software was used to examine the average optical density value (IOD), and the differences in protein-positive expression among the groups were compared.

2.2.12. Statistical analysis

Except for the results of bioinformatics analysis, the results of other analyses were processed using the GraphPad Prism 9.5.1 software (GraphPad, CA, USA). The mean ± standard deviation was used to express quantitative data. One-Way analysis of variance (One-Way ANOVA) was performed for intergroup comparisons. For groups with equal variances, the LSD and student-newman-keuls (SNK) tests were

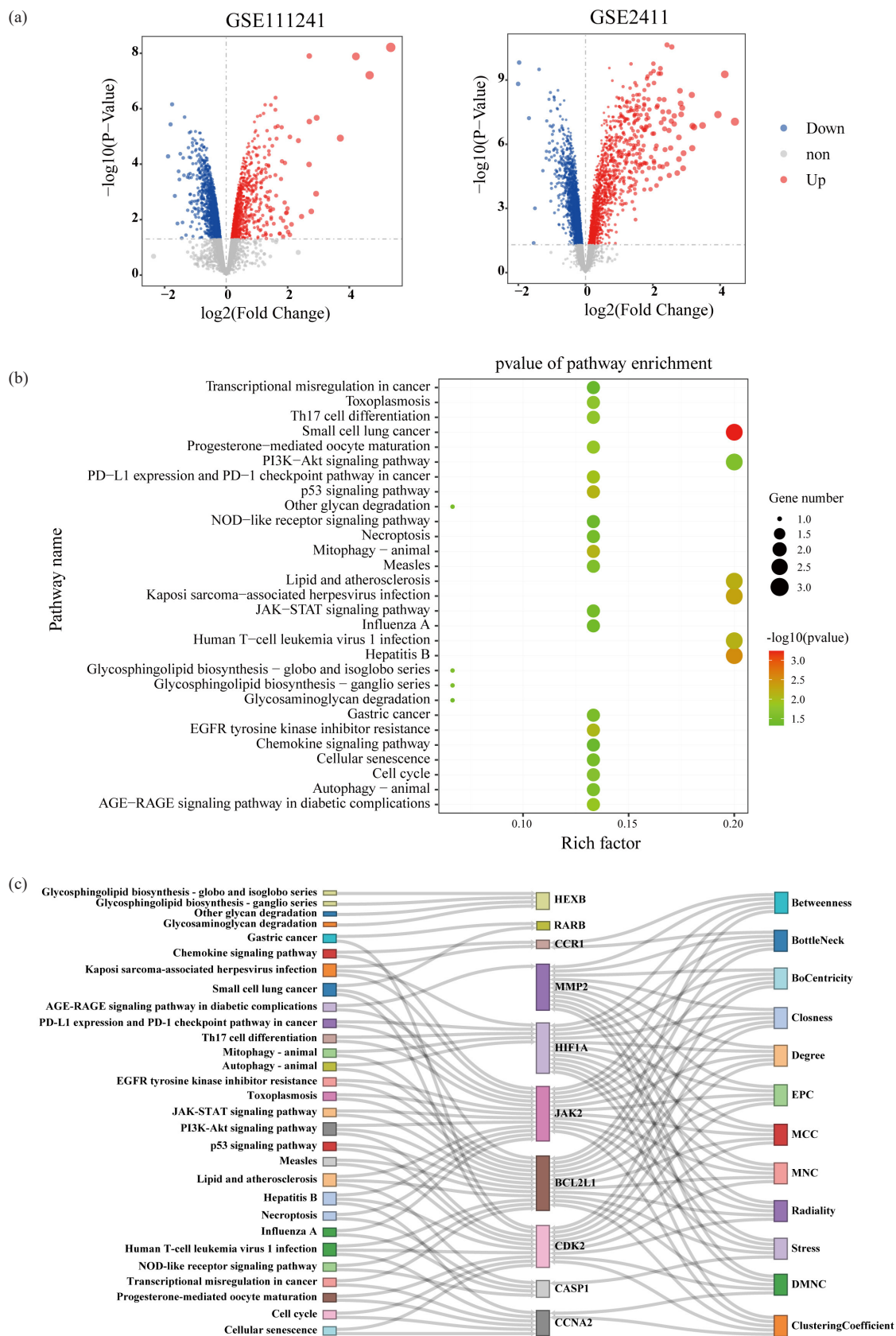


Figure 2. Differential genes and the signaling pathways targeted by LIG to ALI. (a) DEG of ALI in the two datasets, each point in the figure represents a gene; the red marker indicates the upregulated gene, the blue marker indicates the downregulated gene, while the gray marker indicates no DEG. (b) Bubble diagram depicting the KEGG signaling pathway enrichment analysis. LIG targeted 30 DEGs-enriched signaling pathways in ALI; the abscissa of the figure is the Rich factor, while the ordinate is the significantly enriched signaling pathways. The color of the dots in the figure indicates the p-value; the larger the p-value, the darker the color of the dots. The size of the dot represents the number of genes enriched in this pathway; the larger the dot, the greater the number of DEGs enriched in this pathway. (c) LIG targets hub genes in ALI DEGs; in this figure, each signaling pathway is shown on the left; the top 10 hub genes of each algorithm are shown in the middle, and the different algorithms for calculating hub genes are shown on the right.

employed; the Mann–Whitney U-test was used for uneven variance. A statistically significant difference was defined as $P < 0.05$.

3. Results and Discussion

3.1. Differential expression genes of ALI

To obtain the DEGs of ALI and normal control, we performed background correction, standardization, and log2 processing on the original data of GSE111241 and GSE2411, followed by DEG analysis. According to the results, 1331 upregulated genes and 2025 downregulated genes were obtained from GSE111241, and 1643 upregulated genes and 3101 downregulated genes were obtained from GSE2411 (Figure 2a). Considering the shared DEGs as disease target

genes, we finally obtained 1150 genes. These genes were included in the next phase of drug target gene mapping studies to obtain the most likely targets for ALI drug treatment.

3.2. Target genes and enriched pathways of LIG and “LIG-ALI-DEGs” network targeting ALI

SwissTargetPrediction obtained 170 target LIG genes, and PharmMapper obtained 137 target LIG genes. On merging, a total of 164 target LIG genes were obtained. On mapping the target genes to the DEGs of ALI, we found that LIG targets 16 DEGs of ALI, including *Adk*, *Bcl2L1*, *Casp1*, *Ccna2*, *Ccr1*, *Cdk2*, *Glo1*, *HexB*, *Hifla*, *Jak2*, *Lcn2*, *Mmp2*, *Pdk2*, *Rarb*, *Sec14L2*, and *Sult1e1*. These DEGs may be the key effective LIG targets involved in ALI prevention and treatment. Moreover, the

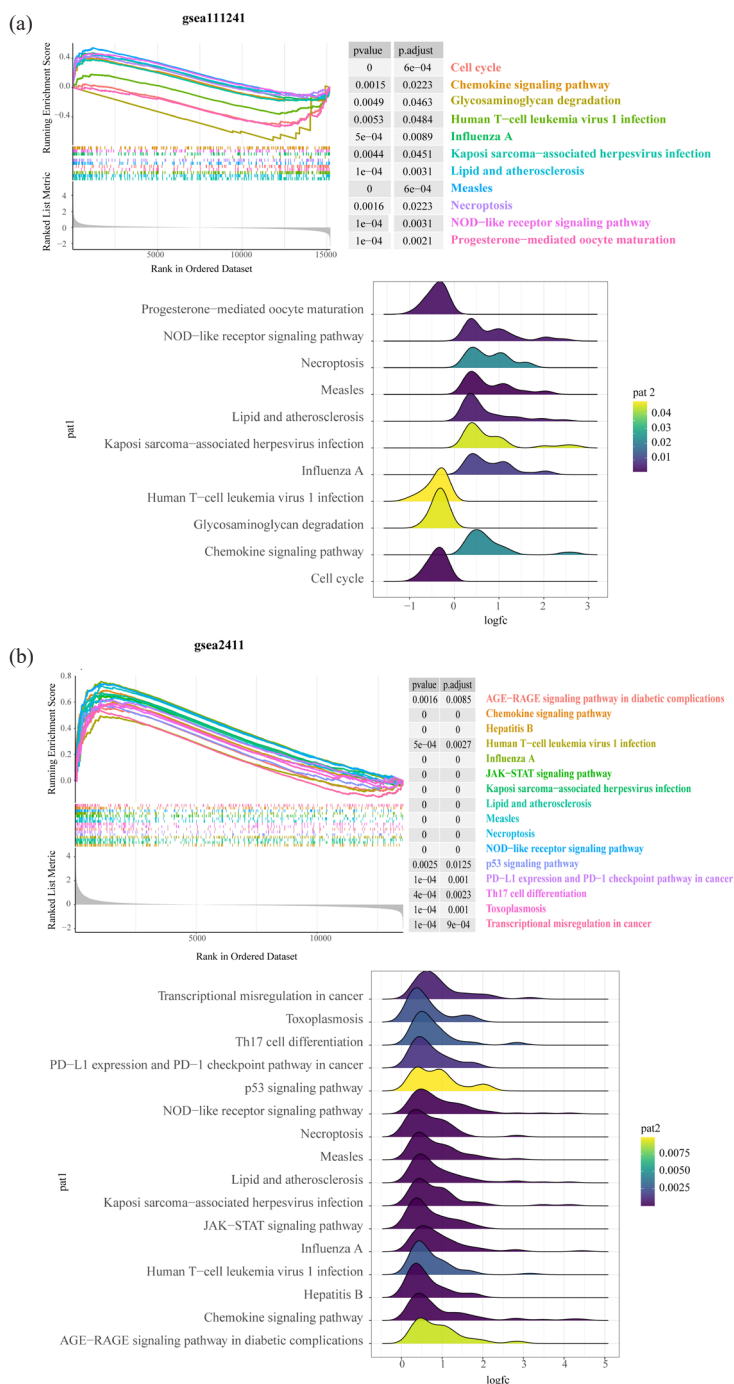


Figure 3. GSEA results of the signaling pathways based on all ALI genes. (a) Significantly enriched pathways and the ridgeline plot in the dataset GSE111241. (b) Significantly enriched pathways and the ridgeline plot in the dataset GSE2411.

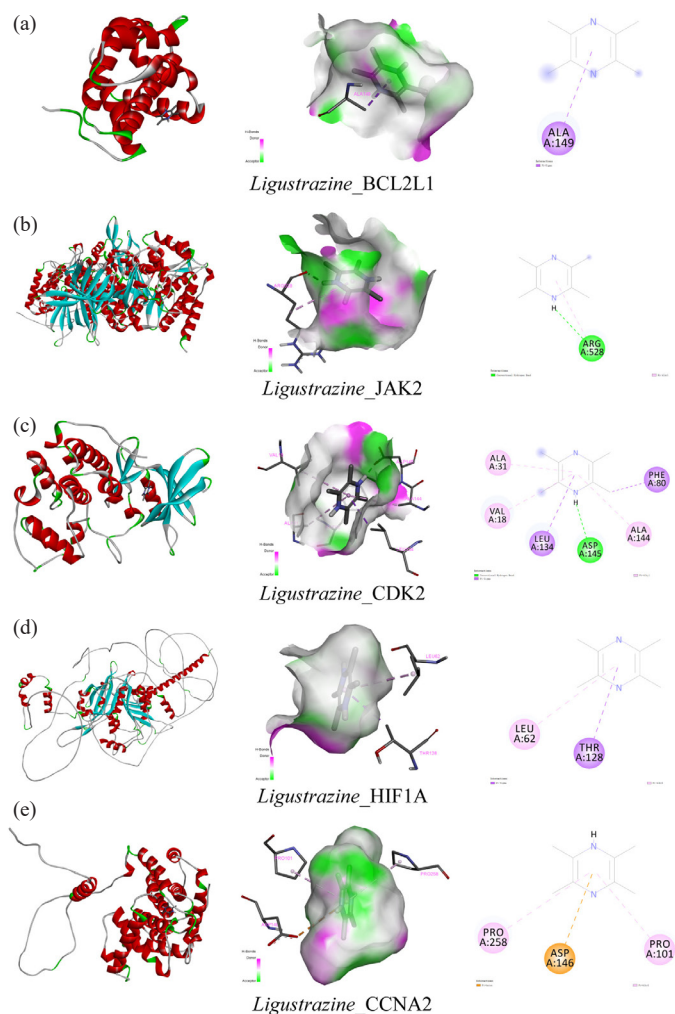
Table 3. Binding energy between *Ligustrazine* and core target protein molecules (kcal/mol).

Protein	BCL2L1	JAK2	CDK2	HIF1A	CCNA2
<i>Ligustrazine</i>	-4.6	-5.2	-5.5	-5.3	-5.5

mechanism behind *LIG* targeting ALI DEGs was examined using the KEGG pathway enrichment analysis, and 30 enriched signaling pathways were identified. Of them, 29 pathways were significantly enriched ($P < 0.05$), including the chemokine, JAK-STAT, and necroptosis (Figure 2b). The hub gene analysis of the genes contained in the top 30 significantly enriched pathways revealed that *BCL2L1*, *Jak2*, *Cdk2*, *Hif1A*, and *Cna2* ranked top 10 in several algorithms (Figure 2c), which were then enriched in multiple signaling pathways.

3.3. GSEA of the signaling pathways

To further confirm whether the KEGG pathway enriched by DEGs plays a role in ALI, the GSEA was performed for all genes in the two datasets. According to the results, the chemokine signaling pathway, NOD-like receptor signaling pathway, and JAK-STAT signaling pathway were significantly enriched ($P < 0.05$) (Figure 3a,b). The JAK-STAT pathway was also identified in the chemokine signaling pathway, which further confirmed that the pathophysiology of ALI was significantly influenced by the JAK-STAT signaling pathway, and *LIG*-mediated targeting of this pathway may be among the key mechanisms for the effect of *LIG*.

**Figure 4.** Visualization of the binding energy between 5 core targets and *LIG*. (a) *BCL2L1*; (b) *JAK2*; (c) *CDK2*; (d) *HIF1A*; (e) *CCNA2*; It was composed of an integrated diagram, a local pocket diagram and a 2D structure diagram.

3.4. The molecular docking results of the target genes and *LIG*

The binding ability of 5 core target proteins to *LIG* was evaluated by Autodock Tools. The decrease in binding energy was concomitant with an enhancement in the stability of the ligand-receptor binding. The binding energy between *BCL2L1* and *LIG* was -4.6 kcal/mol, between *JAK2* and *LIG* was -5.2 kcal/mol, and between *CDK2* and *LIG* was -5.5 kcal/mol. The binding energy between *HIF1A* and *LIG* was -5.3 kcal/mol, and *CCNA2* and *LIG* was -5.5 kcal/mol (Table 3). As shown in Figure 4, *LIG* formed a π - σ interaction with ALA149 in *BCL2L1* (Figure 4a). *LIG* formed a conventional hydrogen bond and π -alkyl interaction with ARG528 in *JAK2* (Figure 4b). In addition, *LIG* formed a Conventional Hydrogen Bond with ASP145 of the *CDK2*; it formed π - σ interactions with PHE80 and LEU134; and it formed π -alkyl interactions with VAL18, ALA31, and ALA144 (Figure 4c). *LIG* formed a π - σ interaction with THR128 and a π -alkyl interaction with LEU62 in *HIF1A* (Figure 4d). Furthermore, *LIG* formed π -anion interaction with ASP146, formed π -alkyl interaction with PRO101 and PRO258 in *CCNA2* (Figure 4e). These results indicate that stable binding structures could be formed between *LIG* and the core targets.

3.5. Effect of *LIG*-OC-COF on inflammatory response in LPS-induced ALI rats

To validate the protective effect of *LIG* in animal models of ALI (Figure 5a), we investigated the lung tissue morphology of the rats (Figure 5b). When compared with the CON group, alveolar shape changes and structural incompleteness were observed in the LPS group. Moreover, inflammatory and red blood cells infiltrated the alveolar cavity and interstitial lung in the LPS group, leading to a markedly higher pathological score. The ALI rat models were thus successfully established. In contrast, drug treatment could significantly reduce the aforementioned pathological damage, and the lung histopathological scores significantly reduced ($P < 0.0001$) (Figure 5c). The *LIG*-OC-COF group had the best effect, exhibiting comparable efficacy to the DEX group. Meanwhile, OC-COF and *LIG* treatment exhibited a certain improvement effect. Moreover, large numbers of neutrophils and macrophages were activated by LPS, which then secrete various inflammatory and chemotactic factors (such as IL-1 β , TNF- α , and IL-6) [24] and reduce the anti-inflammatory component IL-10. The development, growth, and duration of ALI inflammatory responses were influenced by these inflammatory factors as well as other pro-inflammatory substances [25]. Our study's findings supported the previously reported conclusion. TNF- α , IL-6, and IL-1 β levels were significantly higher ($P < 0.0001$), while IL-10 levels were significantly lower ($P < 0.0001$) (Figure 5d-g). Notably, DEX and *LIG*-OC-COF were the most notable therapy effects. These data suggest that *LIG* treatment reversed LPS-induced inflammatory response and that *LIG*-OC-COF further improved efficacy.

3.6. *LIG* plays a protective role in LPS-induced lung tissue damage

TUNEL staining (Figure 6a) revealed that the apoptosis rate significantly increased after LPS intervention. The LPS-induced apoptosis rate was significantly inhibited after treatment with *LIG*, *LIG*-OC-COF, OC-COF, and DEX ($P < 0.0001$) (Figure 6b), while *LIG*-OC-COF exhibited the most significant effect. These results suggest that *LIG*-mediated protection is related to maintaining the lung tissue morphology and attenuating apoptosis.

3.7. Effects of *LIG* on the key target genes and signaling pathways of ALI

Based on the network prediction results, five key target genes were selected for verifying their transcriptional expression levels. LPS could significantly upregulate the expression levels of *BCL2L1*, *JAK2*, *HIF1A*, *CDK2*, and *CCNA2* ($P < 0.0001$) (Figure 7a). However, the transcriptional expression was significantly lower in drug treatment groups. Interestingly, the *LIG*-OC-COF group exhibited a more pronounced level of inhibition of key target gene expression, which was even more effective than those recorded in the DEX group. We investigated the expression levels and phosphorylation status of *JAK2* and the downstream major effector molecule, *STAT3*, in the lung tissue to investigate the JAK/STAT signaling expression.

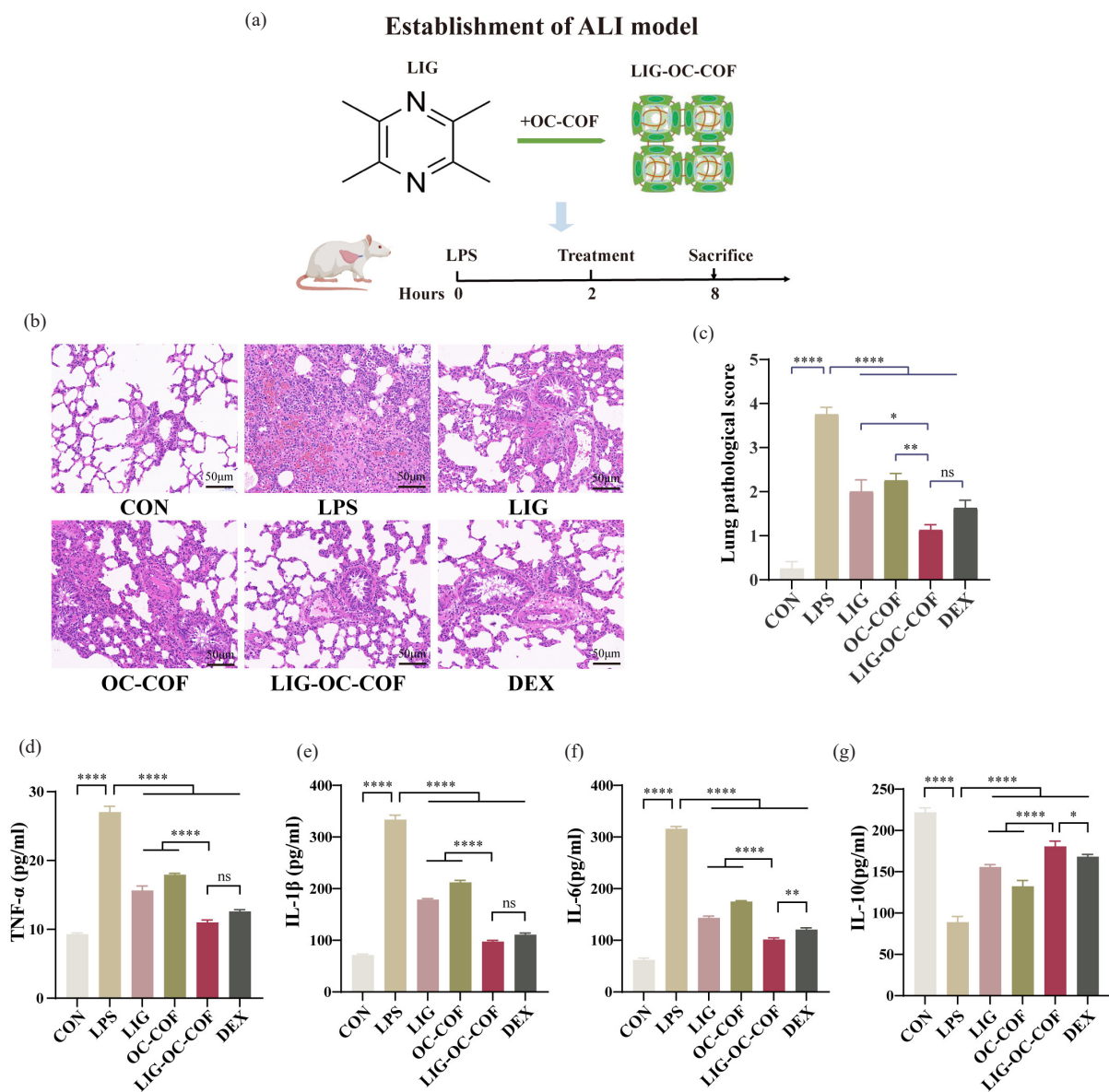


Figure 5. LIG reduced the inflammatory response in ALI model rats. (a) The chemical structure of LIG and the illustration of the experimental treatment of LIG-OC-COF in LPS-induced ALI model rats in each group stained with HE (200×). (b) The lung tissues of rats in each group were scored. (c) The pathological scores of the lung tissues in each group were scored. (d-g) The serum inflammation level in ALI model rats. (d) TNF- α , (e) IL-1 β , (f) IL-6, (g) IL-10. (Averages \pm SD are shown. * P < 0.05, ** P < 0.01, *** P < 0.001, **** P < 0.0001, ns = no significance.)

The results were as we imagined: LPS increased the expression of key target proteins JAK2 and STAT3 and significantly promoted phosphorylation levels (P < 0.0001) (Figure 7b-c), revealing the activation of the signaling pathway. More interestingly, LIG-OC-COF reduced phosphorylation levels of JAK2 and STAT3 (P < 0.0001). Furthermore, the immunohistochemical results also exhibited the same trend (Figure 7d-e). Collectively, these results suggest that LIG exerted the ALI therapeutic effect through the aforementioned key target proteins and the JAK2/STAT3 pathway, with LIG-OC-COF having the most noticeable effect.

3.8. Discussion

ALI develops rapidly and has a high mortality rate. LPS and sepsis are the main pathogenic factors for ALI [26,27]. Overall, ALI pathogenesis is complex involving different interacting molecular pathways [28]. Current therapeutic strategies for ALI primarily focus on preserving pulmonary ventilation function and symptomatic management while specific therapeutic drugs remain clinically unavailable. [29]. Notably, TCM exhibits good clinical efficacy in ALI prevention and treatment

[30,31]. Past studies on various herbal medicines, such as LIG, have also demonstrated protective effects against ALI, such as anti-inflammatory, antioxidant, and antiapoptotic effects [32,33].

LIG is the primary constituent of the TCM *Ligusticum chuanxiiong hort* (Chuan Xiong). LIG has the function of improving microcirculation, regulating immunity, and anti-inflammation [34,35]. However, only a few studies have reported on LIG in ALI treatment, and its relative difficulty is associated with the complexity and diversity of the involved genes and targets. Meanwhile, LIG has limitations, such as short half-life and inadequate oral absorption. Due to the large absorptive surface area and high permeability of the lung tissues, inhalation drug delivery showed significant advantages compared to oral drug delivery. Therefore, network pharmacology and bioinformatics methods were employed to analyze the potential mechanisms of LIG in ALI treatment. Moreover, *in vivo* experiments were conducted by modifying the drug dosage form to validate the effectiveness and action mechanism of LIG. Furthermore, a novel approach to treating ALI with OC-COF as a DPI carrier was put forth.

Network pharmacology analysis identified 16 critical targets (e.g., *Bcl2L1*, *Jak2*, *Cdk2*, *Hif1A*, and *Ccna2*) and 30 pathways implicated in

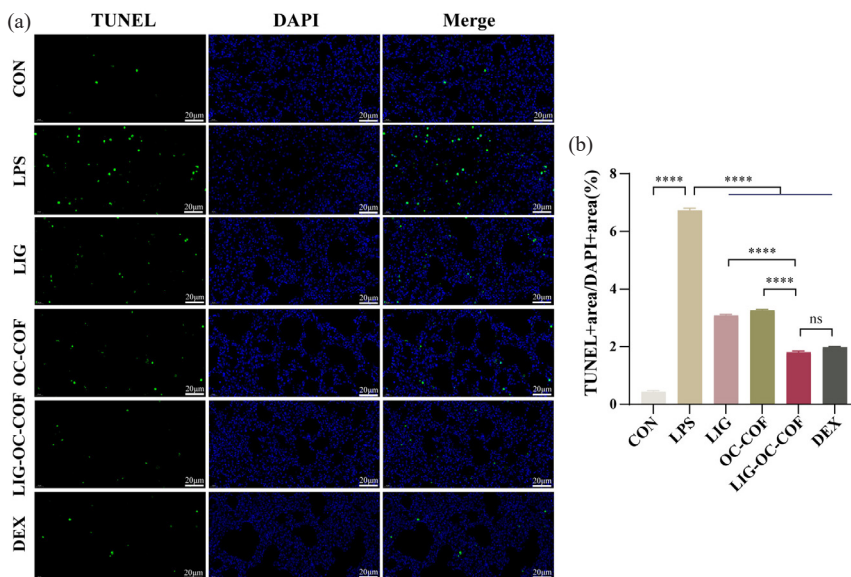


Figure 6. The protective effect of LIG on the lung tissues in ALI model rats. (a) The lung tissues of rats in each group were stained with Tunnell (400×). (b) Percent of TUNEL-positive cells in the lung tissues of rats in each group. (Averages ±SD are shown. **P* < 0.05, ***P* < 0.01, ****P* < 0.001, *****P* < 0.0001, ns = no significance.)

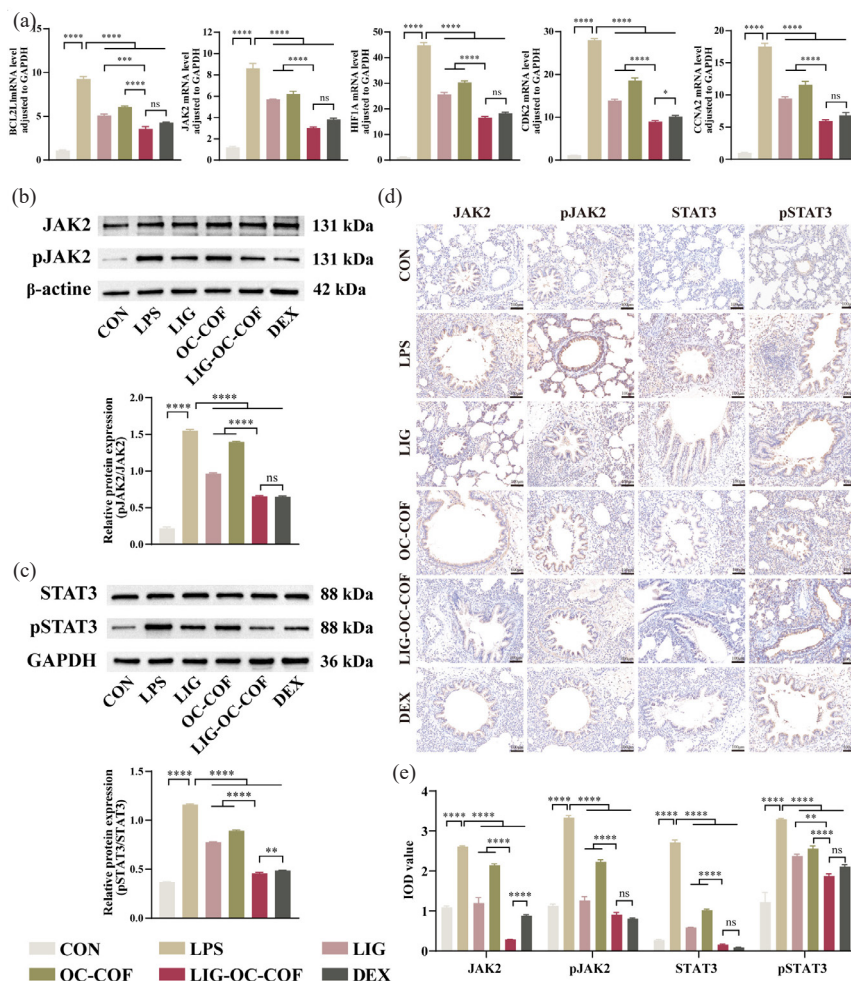


Figure 7. LIG regulated the expression of differential genes and key signaling pathway when stimulated by LPS. (a) The transcriptional expression levels of key target genes BCL2L1, JAK2, HIF1A, CDK2, and CCNA2 in the lung tissues of rats were detected by qRT-PCR; (b-c) The protein expression levels of JAK2, pJAK2, STAT3, and pSTAT3 in the lung tissues of rats were analyzed by western blotting; (d) Immunohistochemical staining of JAK2, pJAK2, STAT3, and pSTAT3 in the lung tissues of rats; (e) IOD values for immunohistochemical staining of the lung tissues in each group of rats, Averages ±SD were shown. **P* < 0.05, ***P* < 0.01, ****P* < 0.001, *****P* < 0.0001, ns = no significance.

inflammation, cell cycle, apoptosis, and oxidative stress regulation. Molecular docking confirmed stable binding affinities between these targets and LIG. Increasing evidence indicates that these targets/pathways are central to ALI pathogenesis [36–39], suggesting LIG exerts anti-ALI effects via multi-mechanistic modulation.

Accordingly, the therapeutic efficacy of LIG was validated in an LPS-induced ALI rat model. LIG showed clear effectiveness in lowering the rats' lung tissue inflammation score and enhancing ALI's inflammatory response, with LIG-OC-COF displaying the most significant effect. The LPS group's lung tissue showed significant congestion and inflammatory cell infiltration. Moreover, there was a marked increase in the levels of serum proinflammatory factors, with a significant decrease in the level of the anti-inflammatory factors. These LPS-induced inflammatory reactions and changes in inflammatory factors could be prevented by LIG, which is consistent with other studies [40]. Additionally, previous pharmacokinetic research has demonstrated that the inhalation dose of LIG, which is one-fifth of the gavage dose, is suitable and equivalent to intragastric delivery [18]. The best therapeutic result was obtained by inhaling LIG-OC-COF, which combined the benefits of LIG with OC-COF and a 5-fold dose reduction, indicating that LIG-OC-COF could improve the activity and bioavailability of LIG. LIG-OC-COF effectively ameliorated the LPS-induced inflammatory response and thus treated ALI.

Among the key targets, CDK2 and CCNA2, are both factors that regulate the cell cycle, which refers to the complete process from the beginning of cell division to new cell generation to the end of the next cell division [41]. If the cell cycle is arrested, the cells cannot proliferate and renew [42,43]. The repair of damage to alveolar epithelial cells necessitates cell proliferation, which depends on the cell cycle circulation. The regulatory cell cycle or related proteins can be used as therapeutic targets for ALI/ARDS [44]. CDK2 is a crucial factor in the cell cycle [45] and has an irreplaceable role in cell proliferation [46], apoptosis [47], differentiation [48], and viral replication and infection [49]. CCNA2 is a regulator of CDK and acts as a binding and activation partner of CDK—a key protein among cell cycle regulatory protein molecules [50]. CDK2 binds to CCNA2 and forms a proteasome complex. This complex can regulate the transition of the cell cycle from G1/S to G2/M [51]. Some studies have also demonstrated that tanshinone (TSA) inhibited pulmonary adenocarcinoma progression by regulating the CCNA2–CDK2 complex [52]. However, only a few studies have reported on the cell cycle in ALI. The present study revealed that LIG could significantly inhibit *CDK2* and *CCNA2* expression in ALI-affected rats, with the inhibitory effect of LIG-OC-COF was the most significant. *Cdk2* and *Ccna2* could be further explored as potential targets for the action of LIG against ALI.

Another important feature of ALI is the apoptosis of alveolar epithelial cells [53]. In our study, a higher apoptosis rate was observed in LPS-induced ALI. Both oral LIG and LIG-OC-COF significantly reduced LPS-induced apoptosis, and the targeted delivery of LIG to the lungs amplified its suppressive effect on apoptosis. In contrast to BCL2-Associated X (BAX), BCL2L1 (BCL-xL) is an anti-apoptotic protein [54]. LPS downregulated the expression of BCL-xL and upregulated the expression of pro-apoptotic proteins BAX and BAK in the ALI mouse models, thereby activating mitochondria-mediated apoptosis [55]. However, in this study, the expression of BCL-xL was upregulated by LPS, while it was downregulated by LIG, suggesting that LIG plays a role in inactivating the apoptotic pathway. Some studies have also demonstrated that CDK2-induced phosphorylation of Ser73 of BCL-xL causes the transformation of BCL-xL into BAX/BAK, which is necessary for inducing cell death [56,57]. In this pathway, apoptosis can be induced even in the absence of additional stress (such as LPS).

ALI is characterized by hypoxemia, acute hypoxic respiratory failure, and systemic inflammatory responses [58]. HIF1A is a class of hypoxia-induced transcription factors. HIF1A is ubiquitinated by von hippel-lindau (VHL) and degraded under normoxia [59], whereas, in a hypoxic environment, it can be involved in regulating physiological processes such as vascular repair, energy metabolism, inflammatory response, apoptosis, and senescence [60]. Multiple studies have demonstrated that HIF1A is a crucial player in ALI. Huang *et al.* reported that the absence of HIF-1 α can reduce pulmonary edema, inflammatory cell accumulation, and inflammatory factor secretion in ALI, thereby offering a treated

effect [61]. TSA IIA (TIIA) improves LPS-induced ALI by reducing HIF-1 α production and enhancing the degradation of phosphatidylinositol-3-kinase/protein kinase B (PI3K/AKT) and Mitogen-activated protein kinase (MAPK) [62]. The study results suggest that LIG reduced the HIF1A expression in the lung tissues and that LIG delivered to the lungs through OC-COF could significantly enhance the efficacy.

To investigate how these target genes are involved, differential genes were enriched through KEGG analysis. The signaling pathways closely related to ALI development in both datasets mainly included the chemokine, nucleotide-binding oligomerization domain (NOD)-like receptor, and JAK-STAT. Further comparative analysis and reference to the KEGG database revealed that the JAK-STAT pathway was also present in the chemokine signaling pathway. JAK2 is among the core targets. Therefore, the key proteins of the JAK-STAT pathway were selected for further experimental validation.

One of the most well-known intracellular signaling networks in inflammatory response is the JAK/STAT pathway. The binding of the cytokines to receptors on the cell membrane can induce phosphorylation of JAK, which then triggers STAT to form dimers and reach the nucleus to control the expression of associated genes. [63]. Among them, JAK2/STAT3 pathway is considered as a classic pathway for transcriptional activation and signal transduction, which plays a crucial role in the progression of ALI [64–66]. LPS-induced inflammatory complexes activate STAT3 and further enhance the inflammatory response, thereby accelerating the ALI progression [67,68]. Hui *et al.* [69] found that JAK2 could be rapidly activated in ALI rats, and its activity in lung tissue peaked at 2 hrs, while STAT3 remained at a high level for up to 48 hrs. SO₂ can protect rats from ALI by inhibiting the JAK2/STAT3 pathway through reducing the level of pSTAT3 [70]. Our research found that LIG prevented LPS from activating the JAK2/STAT3 pathway. Targeting lung delivery with LIG-OC-COF further improved the efficacy of LIG. Additionally, LPS induced the production of IL-6 in both serum and lung tissue, exhibiting a kinetic pattern that aligns with STAT3 activation [71]. This suggests that IL-6 may function as a mediator through which LPS activates JAK2/STAT3. This phenomenon was also found in our results, where the activation of the JAK2/STAT3 pathway was consistent with the expression levels of IL-6 [72]. Therefore, effective ALI treatment could be achieved by modulating the JAK2/STAT3 signal transduction.

Collectively, these data suggested that LIG-OC-COF exerted significant efficacy. When combined with the special physiology of lung tissues, LIG is loaded into OC-COF, which is used as a DPI LIG-OC-COF to deliver LIG directly into the deep alveoli. LIG-OC-COF can downregulate IL-6, IL-1 β , and TNF- α expression in the serum of ALI rats, upregulate IL-10 expression, and reduce the BCL2L1, JAK2, HIF1A, CDK2, and CCNA2 mRNA transcript levels in the lung tissues and regulate the expression of JAK-STAT3 pathway-related proteins. This finding enhances the efficacy of LIG. Meanwhile, LIG plays a role in systemic therapy, which offers good support for the clinical application of LIG-OC-COF.

4. Conclusions

This study analyzed the potential mechanism underlying the anti-ALI action of LIG using network pharmacology and bioinformatics. We found that LIG may improve the lung injury situation by regulating the cell cycle, anti-apoptosis, anti-inflammatory, and antioxidative stress processes and modulating the JAK2/STAT3 signaling pathway to exert its anti-ALI effects. LIG-OC-COF-targeted lung delivery significantly improved efficacy relative to oral LIG administration. Overall, LIG-OC-COF demonstrated great potential as a novel drug delivery system for the clinical treatment of ALI. However, only key molecules were verified in this study, and further discussion on the *in vitro* mechanism and clinical research is warranted. Moreover, other specific mechanisms need further exploration.

CRedit authorship contribution statement

Zegeng Li: Conceived the experimental idea and was responsible for the final review and revision. **Di Wu:** Completed the experimental part, organized and analyzed the data, wrote the article. **Xiaole**

Wang: Organized and analyzed the data. **Yu Jia, Qinjun Yang, and Huanzhang Ding:** Completed the experimental part. **Siyu He:** Prepared the experimental drug. **Yating Gao:** Designed the experimental method. **Tong Liu and Mengyao Shi:** Processed and analyzed the data. **Jie Zhu:** Was responsible for the final review and revision. **Jiwen Zhang:** Conceived the experimental idea. All authors read and approved the final article.

Declaration of competing interest

The authors declare that they have no known competing financial interests or personal relationships that could have influenced the work reported in this paper.

Declaration of Generative AI and AI-assisted technologies in the writing process

The authors confirm that there was no use of artificial intelligence (AI)-assisted technology for assisting in the writing or editing of the manuscript and no images were manipulated using AI.

Acknowledgment

This work was supported by the National Key R&D Program of China (no. 2020YFE0201700), the National Natural Science Foundation of China, the Joint Fund for Regional Innovation and Development (no. U20A20398), the Natural Science Foundation Project of Anhui Province (no. 2208085QH264) and the Anhui University Collaborative Innovation Project, China (no. GXXT-2020-025). We are grateful to the Center for Drug Delivery Systems, Shanghai Institute of Materia Medica, and Chinese Academy of Science for the LIG-OC-COF.

References

- Ning, L., Shishi, Z., Bo, W., Huiqing, L., 2023. Targeting immunometabolism against acute lung injury. *Clinical Immunology*, **249**, 109289. <https://doi.org/10.1016/j.clim.2023.109289>
- Ding, Z., Zhong, R., Yang, Y., Xia, T., Wang, W., Wang, Y., Xing, N., Luo, Y., Li, S., Shang, L., Shu, Z., 2020. Systems pharmacology reveals the mechanism of activity of ge-ge-qin-lian decoction against LPS-induced acute lung injury: A novel strategy for exploring active components and effective mechanism of TCM formulae. *Pharmacological Research*, **156**, 104759. <https://doi.org/10.1016/j.phrs.2020.104759>
- Dutta, S., Zhu, Y., Han, Y., Almuntashiri, S., Wang, X., Zhang, D., 2023. Long noncoding RNA: A novel insight into the pathogenesis of acute lung injury. *Journal of Clinical Medicine*, **12**, 604. <https://doi.org/10.3390/jcm12020604>
- Zhu, Y., Han, Q., Wang, L., Wang, B., Chen, J., Cai, B., Wu, C., Zhu, X., Liu, F., Han, D., Dong, H., Jia, Y., Liu, Y., 2023. Jinhua qinggan granules attenuates acute lung injury by promotion of neutrophil apoptosis and inhibition of TLR4/MyD88/NF- κ B pathway. *Journal of Ethnopharmacology*, **301**, 115763. <https://doi.org/10.1016/j.jep.2022.115763>
- Min, S., Tao, W., Ding, D., Zhang, X., Zhao, S., Zhang, Y., Liu, X., Gao, K., Liu, S., Li, L., Hou, M., Li, Y., 2023. Tetramethylpyrazine ameliorates acute lung injury by regulating the Rac1/LIMK1 signaling pathway. *Frontiers in Pharmacology*, **13**, 1005014. <https://doi.org/10.3389/fphar.2022.1005014>
- Wang, Y., Zhu, H., Tong, J., Li, Z., 2022. Ligustrazine inhibits lung phosphodiesterase activity in a rat model of allergic asthma. *Computational and Mathematical Methods in Medicine*, **2022**, 1452116. <https://doi.org/10.1155/2022/1452116>
- Lin, J., Wang, Q., Zhou, S., Xu, S., Yao, K., 2022. Tetramethylpyrazine: A review on its mechanisms and functions. *Biomedicine & Pharmacotherapy = Biomedicine & Pharmacotherapie*, **150**, 113005. <https://doi.org/10.1016/j.biopha.2022.113005>
- Lian, N., Tong, J., Zhu, W., Meng, Q., Jiang, M., Bian, M., Li, Y., 2023. Ligustrazine and liguzinediol protect against doxorubicin-induced cardiomyocytes injury by inhibiting mitochondrial apoptosis and autophagy. *Clinical and Experimental Pharmacology & Physiology*, **50**, 867-877. <https://doi.org/10.1111/1440-1681.13811>
- Yanyu, X., Qineng, P., Zhigui, S., Hongying, L., Jiangxiu, N., 2012. Preparation and pharmacokinetics in beagle dogs of once-a-day tetramethylpyrazine phosphate sustained-release pellets. *Drug Development and Industrial Pharmacy*, **38**, 301-6. <https://doi.org/10.3109/03639045.2011.602408>
- Alipour, S., Mahmoudi, L., Ahmadi, F., 2023. Pulmonary drug delivery: An effective and convenient delivery route to combat COVID-19. *Drug Delivery and Translational Research*, **13**, 705-715. <https://doi.org/10.1007/s13346-022-01251-1>
- Chen, Y., Yu, B., Xu, S., Ma, F., Gong, J., 2019. Core-shell-structured cyclodextrin metal-organic frameworks for programmable cargo release. *ACS Applied Materials & Interfaces*, **11**, 16280-4. <https://doi.org/10.1021/acsami.9b01040>
- Hamedi, A., Anceschi, A., Patrucco, A., Hasanzadeh, M., 2022. A γ -cyclodextrin-based metal-organic framework (γ -CD-MOF): A review of recent advances for drug delivery application. *Journal of Drug Targeting*, **30**, 381-393. <https://doi.org/10.1080/1061186x.2021.2012683>
- Liu, B., Li, H., Xu, X., Li, X., Lv, N., Singh, V., Stoddart, J.F., York, P., Xu, X., Gref, R., Zhang, J., 2016. Optimized synthesis and crystalline stability of γ -cyclodextrin metal-organic frameworks for drug adsorption. *International Journal of Pharmaceutics*, **514**, 212-9. <https://doi.org/10.1016/j.ijpharm.2016.09.029>
- Hartlieb, K.J., Ferris, D.P., Holcroft, J.M., Kandela, I., Stern, C.L., Nassar, M.S., Botros, Y.Y., Stoddart, J.F., 2017. Encapsulation of ibuprofen in CD-MOF and related bioavailability studies. *Molecular Pharmaceutics*, **14**, 1831-1839. <https://doi.org/10.1021/acs.molpharmaceut.7b00168>
- Li, H., Lv, N., Li, X., Liu, B., Feng, J., Ren, X., Guo, T., Chen, D., Fraser Stoddart, J., Gref, R., Zhang, J., 2017. Composite CD-MOF nanocrystals-containing microspheres for sustained drug delivery. *Nanoscale*, **9**, 7454-7463. <https://doi.org/10.1039/c6nr07593b>
- Li, H., Zhu, J., Wang, C., Qin, W., Hu, X., Tong, J., Yu, L., Zhang, G., Ren, X., Li, Z., Zhang, J., 2020. Paeonol loaded cyclodextrin metal-organic framework particles for treatment of acute lung injury via inhalation. *International Journal of Pharmaceutics*, **587**, 119649. <https://doi.org/10.1016/j.ijpharm.2020.119649>
- Singh, V., Guo, T., Xu, H., Wu, L., Gu, J., Wu, C., Gref, R., Zhang, J., 2017. Moisture resistant and biofriendly CD-MOF nanoparticles obtained via cholesterol shielding. *Chemical Communications (Cambridge, England)*, **53**, 9246-9. <https://doi.org/10.1039/c7cc03471g>
- He, S., Wu, L., Sun, H., Wu, D., Wang, C., Ren, X., Shao, Q., York, P., Tong, J., Zhu, J., Li, Z., Zhang, J., 2022. Antioxidant biodegradable covalent cyclodextrin frameworks as particulate carriers for inhalation therapy against acute lung injury. *ACS Applied Materials & Interfaces*, **14**, 38421-38435. <https://doi.org/10.1021/acscami.2c05220>
- Ritchie, M.E., Phipson, B., Wu, D., Hu, Y., Law, C.W., Shi, W., Smyth, G.K., 2015. limma powers differential expression analyses for RNA-sequencing and microarray studies. *Nucleic acids research*, **43**, e47. <https://doi.org/10.1093/nar/gkv007>
- Yu, G., Wang, L.-G., Han, Y., He, Q.-Y., 2012. clusterProfiler: An R package for comparing biological themes among gene clusters. *OMICS: A Journal of Integrative Biology*, **16**, 284-7. <https://doi.org/10.1089/omi.2011.0118>
- McGuigan, R.M., Mullenix, P., Norlund, L.L., Ward, D., Walts, M., Azarow, K., 2003. Acute lung injury using oleic acid in the laboratory rat: Establishment of a working model and evidence against free radicals in the acute phase. *Current Surgery*, **60**, 412-7. [https://doi.org/10.1016/S0149-7944\(02\)00775-4](https://doi.org/10.1016/S0149-7944(02)00775-4)
- Wang, X., Shen, Y., Zhuang, X., Wang, N., Zhang, Q., Zhu, L., Liu, Y., Lu, X., Qin, L., Zhang, Q., 2021. Jintiang capsule alleviates rheumatoid arthritis and reverses changes of serum metabolic profile in collagen-induced arthritic rats. *Journal of Inflammation Research*, **14**, 6685-6706. <https://doi.org/10.2147/JIR.S338107>
- Li, X., Hong, G., Zhao, G., Pei, H., Qu, J., Chun, C., Huang, Z., Lu, Z., 2022. Red blood cell membrane-camouflaged PLGA nanoparticles loaded with basic fibroblast growth factor for attenuating sepsis-induced cardiac injury. *Frontiers in Pharmacology*, **13**, 881320. <https://doi.org/10.3389/fphar.2022.881320>
- Wang, W.B., Li, J.T., Hui, Y., Shi, J., Wang, X.Y., Yan, S.G., 2022. Combination of pseudoephedrine and emodin ameliorates LPS-induced acute lung injury by regulating macrophage M1/M2 polarization through the VIP/cAMP/PKA pathway. *Chinese Medicine*, **17**, 19. <https://doi.org/10.1186/s13020-021-00562-8>
- Wang, S., Lin, F., Zhang, C., Gao, D., Qi, Z., Wu, S., Wang, W., Li, X., Pan, L., Xu, Y., Tan, B., Yang, A., 2024. Xuanbai chengqi decoction alleviates acute lung injury by inhibiting NLRP3 inflammasome. *Journal of Ethnopharmacology*, **319**, 117227. <https://doi.org/10.1016/j.jep.2023.117227>
- Grégoire, M., Uhel, F., Lesouhaitier, M., Gacouin, A., Guirriec, M., Mourcin, F., Dumontet, E., Chalin, A., Samson, M., Berthelot, L.L., Tissot, A., Kerjouan, M., Jouneau, S., Le Tulzo, Y., Tarte, K., Zmijewski, J.W., Tadié, J.M., 2018. Impaired efferocytosis and neutrophil extracellular trap clearance by macrophages in ARDS. *The European Respiratory Journal*, **52**, 1702590. <https://doi.org/10.1183/13993003.02590-2017>
- Yan, Z., Ji, F., Yan, R., Jiao, J., Wang, W., Zhang, M., Li, F., Zhao, Y., Chang, Z., Yan, S., Li, J., 2024. Reyanning mixture inhibits M1 macrophage polarization through the glycogen synthesis pathway to improve lipopolysaccharide-induced acute lung injury. *Journal of Ethnopharmacology*, **328**, 118005. <https://doi.org/10.1016/j.jep.2024.118005>
- Mowery, N.T., Terzian, W.T.H., Nelson, A.C., 2020. Acute lung injury. *Current Problems in Surgery*, **57**, 100777. <https://doi.org/10.1016/j.cpsurg.2020.100777>
- Derwall, M., Martin, L., Rossaint, R., 2018. The acute respiratory distress syndrome: Pathophysiology, current clinical practice, and emerging therapies. *Expert Review of Respiratory Medicine*, **12**, 1021-9. <https://doi.org/10.1080/17476348.2018.1548280>
- Guo, J., Zhu, J., Wang, Q., Wang, J., Jia, Y., 2021. Comparative efficacy of seven kinds of chinese medicine injections in acute lung injury and acute respiratory distress syndrome: A network meta-analysis of randomized controlled trials. *Frontiers in Pharmacology*, **12**, 627751. <https://doi.org/10.3389/fphar.2021.627751>
- Zhengqiu, Y. U., Y. U. Liuda, C. Ye, L. I. Mingjing and C. Wanru, 2024. Effectiveness and safety of Qidong Huoxue decoction in treatment of acute lung injury and acute respiratory distress syndrome: a randomized, controlled trial. *J Tradit Chin Med*, **44**, 381-7. <https://doi.org/10.19852/j.cnki.jtcm.2024.02.003>
- Tang, T., Wang, F., Liu, J., Ye, W., Zhao, T., Li, Z., 2022. Rhubarb alleviates acute lung injury by modulating gut microbiota dysbiosis in mice. *Current Microbiology*, **79**, 116. <https://doi.org/10.1007/s00284-022-02811-x>
- Li, S., Xu, Y., He, S., Li, X., Shi, J., Zhang, B., Zhu, Y., Li, X., Wang, Y., Liu, C., Ma, Y., Dong, S., Yu, J., 2023. Tetramethylpyrazine ameliorates endotoxin-induced acute lung injury by relieving golgi stress via the Nrf2/HO-1 signaling pathway. *BMC Pulmonary Medicine*, **23**, 286. <https://doi.org/10.1186/s12890-023-02585-3>
- Huang, H., Kong, L., Luan, S., Qi, C., Wu, F., 2021. Ligustrazine suppresses platelet-derived growth factor-BB-induced pulmonary artery smooth muscle cell proliferation and inflammation by regulating the PI3K/AKT signaling pathway.

- The American Journal of Chinese Medicine*, 49, 437-459. <https://doi.org/10.1142/S0192415X21500208>
35. Gao, J., Ren, J., Ma, X., Zhang, Y., Song, L., Liu, J., Shi, D., Ma, X., 2022. Ligustrazine prevents coronary microcirculation dysfunction in rats via suppression of miR-34a-5p and promotion of Sirt1. *European Journal of Pharmacology*, 929, 175150. <https://doi.org/10.1016/j.ejphar.2022.175150>
 36. Zhao, J., Yu, H., Liu, Y., Gibson, S.A., Yan, Z., Xu, X., Gaggari, A., Li, P.K., Li, C., Wei, S., Benveniste, E.N., Qin, H., 2016. Protective effect of suppressing STAT3 activity in LPS-induced acute lung injury. *American Journal of Physiology. Lung Cellular and Molecular Physiology*, 311, L868-L880. <https://doi.org/10.1152/ajplung.00281.2016>
 37. Keskinidou, C., Lotsios, N.S., Vassiliou, A.G., Dimopoulou, I., Kotanidou, A., Orfanos, S.E., 2022. The interplay between aquaporin-1 and the hypoxia-inducible factor 1 α in a lipopolysaccharide-induced lung injury model in human pulmonary microvascular endothelial cells. *International Journal of Molecular Sciences*, 23, 10588. <https://doi.org/10.3390/ijms231810588>
 38. Nežić, L., Amidžić, L., Škrbić, R., Gajanin, R., Mandić, D., Dumanović, J., Milovanović, Z., Jačević, V., 2022. Amelioration of endotoxin-induced acute lung injury and alveolar epithelial cells apoptosis by simvastatin is associated with up-regulation of survivin/NF- κ B/p65 pathway. *International Journal of Molecular Sciences*, 23, 2596. <https://doi.org/10.3390/ijms23052596>
 39. Xiao, S., Liu, L., Sun, Z., Liu, X., Xu, J., Guo, Z., Yin, X., Liao, F., Xu, J., You, Y., Zhang, T., 2022. Network pharmacology and experimental validation to explore the mechanism of qing-jin-hua-tan-decoction against acute lung injury. *Frontiers in Pharmacology*, 13, 891889. <https://doi.org/10.3389/fphar.2022.891889>
 40. Jiang, R., Xu, J., Zhang, Y., Zhu, X., Liu, J., Tan, Y., 2021. Ligustrazine alleviate acute lung injury through suppressing pyroptosis and apoptosis of alveolar macrophages. *Frontiers in Pharmacology*, 12, 680512. <https://doi.org/10.3389/fphar.2021.680512>
 41. Gao, S., Tan, H., Gang, J., 2024. Inhibition of hepatocellular carcinoma cell proliferation through regulation of the cell cycle, AGE-RAGE, and leptin signaling pathways by a compound formulation comprised of andrographolide, wogonin, and oroxylin A derived from andrographis paniculata(Burm.f.) nees. *Journal of Ethnopharmacology*, 329, 118001. <https://doi.org/10.1016/j.jep.2024.118001>
 42. Zhang, C., Quan, Y., Yang, L., Bai, Y., Yang, Y., 2022. 6-methoxyflavone induces s-phase arrest through the CCNA2/CDK2/p21CIP1 signaling pathway in heLa cells. *Bioengineered*, 13, 7277-7292. <https://doi.org/10.1080/21655979.2022.2047496>
 43. Li, J., Shang, L., Zhou, F., Wang, S., Liu, N., Zhou, M., Lin, Q., Zhang, M., Cai, Y., Chen, G., Yang, S., 2023. Herba patriniae and its component isovitexin show anti-colorectal cancer effects by inducing apoptosis and cell-cycle arrest via p53 activation. *Biomedicine & Pharmacotherapy = Biomedicine & Pharmacotherapie*, 168, 115690. <https://doi.org/10.1016/j.biopha.2023.115690>
 44. Wang, M., Yan, J., He, X., Zhong, Q., Zhan, C., Li, S., 2016. Candidate genes and pathogenesis investigation for sepsis-related acute respiratory distress syndrome based on gene expression profile. *Biological Research*, 49, 25. <https://doi.org/10.1186/s40659-016-0085-4>
 45. Arora, M., Moser, J., Hoffman, T.E., Watts, L.P., Min, M., Musteanu, M., Rong, Y., Ill, C.R., Nangia, V., Schneider, J., Sanclemente, M., Lapek, J., Nguyen, L., Niessen, S., Dann, S., VanArsdale, T., Barbacid, M., Miller, N., Spencer, S.L., 2023. Rapid adaptation to CDK2 inhibition exposes intrinsic cell-cycle plasticity. *Cell*, 186, 2628-2643. <https://doi.org/10.1016/j.cell.2023.05.013>
 46. Tsoo, C.-H., Hsieh, W.-C., Yang, R.-Y., Lo, Y.-H., Tu, T.-J., Ke, L.-Y., Zouboulis, C.C., Liu, F.-T., 2022. Galectin-12 modulates sebocyte proliferation and cell cycle progression by regulating cyclin A1 and CDK2. *Glycobiology*, 32, 73-82. <https://doi.org/10.1093/glycob/cwab100>
 47. Zhu, L., Wang, Y., Lv, W., Wu, X., Sheng, H., He, C., Hu, J., 2021. Schizandrin A can inhibit non-small cell lung cancer cell proliferation by inducing cell cycle arrest, apoptosis and autophagy. *International Journal of Molecular Medicine*, 48, 214. <https://doi.org/10.3892/ijmm.2021.5047>
 48. Haussmann, I.U., Bodi, Z., Sanchez-Moran, E., Mongan, N.P., Archer, N., Fray, R.G., Soller, M., 2016. m6A potentiates sxl alternative pre-mRNA splicing for robust drosophila sex determination. *Nature*, 540, 301-4. <https://doi.org/10.1038/nature20577>
 49. Guo, S., Lei, X., Chang, Y., Zhao, J., Wang, J., Dong, X., Liu, Q., Zhang, Z., Wang, L., Yi, D., Ma, L., Li, Q., Zhang, Y., Ding, J., Liang, C., Li, X., Guo, F., Wang, J., Cen, S., 2022. SARS-coV-2 hijacks cellular kinase CDK2 to promote viral RNA synthesis. *Signal Transduction and Targeted Therapy*, 7, 400. <https://doi.org/10.1038/s41392-022-01239-w>
 50. Loukil, A., Izard, F., Georgieva, M., Mashayekhan, S., Blanchard, J.M., Parmeggiani, A., Peter, M., 2016. Foci of cyclin A2 interact with actin and rhoA in mitosis. *Scientific Reports*, 6, 27215. <https://doi.org/10.1038/srep27215>
 51. Wu, J., Lv, Q., He, J., Zhang, H., Mei, X., Cui, K., Huang, N., Xie, W., Xu, N., Zhang, Y., 2014. MicroRNA-188 suppresses G1/S transition by targeting multiple cyclin/CDK complexes. *Cell Communication and Signaling : CCS*, 12, 66. <https://doi.org/10.1186/s12964-014-0066-6>
 52. Li, Z., Zhang, Y., Zhou, Y., Wang, F., Yin, C., Ding, L., Zhang, S., 2021. Tanshinone IIA suppresses the progression of lung adenocarcinoma through regulating CCNA2-CDK2 complex and AURKA/PLK1 pathway. *Scientific Reports*, 11, 23681. <https://doi.org/10.1038/s41598-021-0166-2>
 53. Li, N., Liu, B., Xiong, R., Li, G., Wang, B., Geng, Q., 2023. HDAC3 deficiency protects against acute lung injury by maintaining epithelial barrier integrity through preserving mitochondrial quality control. *Redox Biology*, 63, 102746. <https://doi.org/10.1016/j.redox.2023.102746>
 54. Li, M., Wang, D., He, J., Chen, L., Li, H., 2020. Bcl-XL: A multifunctional anti-apoptotic protein. *Pharmacological Research*, 151, 104547. <https://doi.org/10.1016/j.phrs.2019.104547>
 55. Lv, X., Lu, X., Zhu, J., Wang, Q., 2020. Lipopolysaccharide-induced acute lung injury is associated with increased ran-binding protein in microtubule-organizing center (RanBPM) molecule expression and mitochondria-mediated apoptosis signaling pathway in a mouse model. *Medical Science Monitor : International Medical Journal of Experimental and Clinical Research*, 26, e923172. <https://doi.org/10.12659/MSM.923172>
 56. Megyesi, J., Tarcsafalvi, A., Seng, N., Hodeify, R., Price, P.M., 2016. Cdk2 phosphorylation of bcl-xL after stress converts it to a pro-apoptotic protein mimicking bax/Bak. *Cell Death Discovery*, 2, 15066. <https://doi.org/10.1038/cddiscovery.2015.66>
 57. Seng, N.S., Megyesi, J., Tarcsafalvi, A., Price, P.M., 2016. Mimicking Cdk2 phosphorylation of bcl-xL at Ser73 results in caspase activation and bcl-xL cleavage. *Cell Death Discovery*, 2, 16001. <https://doi.org/10.1038/cddiscovery.2016.1>
 58. Zhou, M., Meng, L., He, Q., Ren, C., Li, C., 2024. Valsartan attenuates LPS-induced ALI by modulating NF- κ B and MAPK pathways. *Frontiers in Pharmacology*, 15. <https://doi.org/10.3389/fphar.2024.1321095>
 59. Meyers, L. M., C. Krawic, M. W. Luczak and A. Zhitkovich, 2022. Vulnerability of HIF1 α and HIF2 α to damage by proteotoxic stressors. *Toxicol Appl Pharmacol*. 445, 116041. <https://doi.org/10.1016/j.taap.2022.116041>
 60. Copeland C.A., Olenchock B.A., Ziehr D., McGarrity S., Leahy K., Young J.D., Loscalzo J., Oldham W.M., 2023. MYC overrides HIF-1 α to regulate proliferating primary cell metabolism in hypoxia. *eLife*, 12, e82597. <https://doi.org/10.7554/eLife.82597>
 61. Huang, Y., Zhao, C., Chen, J., Su, X., 2018. Deficiency of HIF-1 α in myeloid cells protects escherichia coli or LPS-induced acute lung injury. *QJM: An International Journal of Medicine*, 111, 707-714. <https://doi.org/10.1093/qjmed/hcy160>
 62. Xu, M., Cao, F., Liu, L., Zhang, B., Wang, Y., Dong, H., Cui, Y., Dong, M., Xu, D., Liu, Y., Zhao, P., Niu, W., Li, Z., 2011. Tanshinone IIA-Induced attenuation of lung injury in endotoxemic mice is associated with reduction of hypoxia-inducible factor 1 α expression. *American Journal of Respiratory Cell and Molecular Biology*, 45, 1028-1035. <https://doi.org/10.1165/rcmb.2011-0113oc>
 63. Xin, P., Xu, X., Deng, C., Liu, S., Wang, Y., Zhou, X., Ma, H., Wei, D., Sun, S., 2020. The role of JAK/STAT signaling pathway and its inhibitors in diseases. *International Immunopharmacology*, 80, 106210. <https://doi.org/10.1016/j.intimp.2020.106210>
 64. Yu, Y., Zhu, T., Li, Y., Jing, L., Yang, M., Li, Y., Duan, J., Sun, Z., 2019. Repeated intravenous administration of silica nanoparticles induces pulmonary inflammation and collagen accumulation via JAK2/STAT3 and TGF- β /Smad3 pathways in vivo. *International Journal of Nanomedicine*, 14, 7237-7247. <https://doi.org/10.2147/ijn.s209458>
 65. Cao, F., Tian, X., Li, Z., Lv, Y., Han, J., Zhuang, R., Cheng, B., Gong, Y., Ying, B., Jin, S., Gao, Y., 2020. Suppression of NLRP3 inflammasome by erythropoietin via the EPOR/JAK2/STAT3 pathway contributes to attenuation of acute lung injury in mice. *Frontiers in Pharmacology*, 11, 306. <https://doi.org/10.3389/fphar.2020.00306>
 66. Cai, M., Ye, H., Zhu, X., Li, X., Cai, L., Jin, J., Chen, Q., Shi, Y., Yang, L., Wang, L., Huang, X., 2024. Fibroblast growth factor 21 relieves lipopolysaccharide-induced acute lung injury by suppressing JAK2/STAT3 signaling pathway. *Inflammation*, 47, 209-226. <https://doi.org/10.1007/s10753-023-01905-3>
 67. Xu, F., Wang, S., Wang, Y., Hu, L., Zhu, L., 2023. Inhibition of gp130 alleviates LPS-induced lung injury by attenuating apoptosis and inflammation through JAK1/STAT3 signaling pathway. *Inflammation Research : Official Journal of the European Histamine Research Society ... [et al.]*, 72, 493-507. <https://doi.org/10.1007/s00011-022-01686-9>
 68. Yang, J., Chen, X., 2023. SIRT6 attenuates LPS-induced inflammation and apoptosis of lung epithelial cells in acute lung injury through ACE2/STAT3/PIM1 signaling. *Immunity, Inflammation and Disease*, 11, e809. <https://doi.org/10.1002/iid3.809>
 69. Hui, L., Yao, Y., Wang, S., Yu, Y., Dong, N., Li, H., Sheng, Z., 2009. Inhibition of janus kinase 2 and signal transduction and activator of transcription 3 protect against cecal ligation and puncture-induced multiple organ damage and mortality. *The Journal of Trauma*, 66, 859-865. <https://doi.org/10.1097/TA.0b013e318164d05f>
 70. Zhao, Y.R., Wang, D., Liu, Y., Shan, L., Zhou, J.L., 2016. The PI3K/Akt, p38MAPK, and JAK2/STAT3 signaling pathways mediate the protection of SO2 against acute lung injury induced by limb ischemia/reperfusion in rats. *The Journal of Physiological Sciences : JPS*, 66, 229-239. <https://doi.org/10.1007/s12576-015-0418-z>
 71. Piao, X., Zou, Y., Sui, X., Liu, B., Meng, F., Li, S., Zhang, Q., Ma, C., Wu, T., 2019. Hydrostatin-SN10 ameliorates pancreatitis-induced lung injury by affecting IL-6-induced JAK2/STAT3-associated inflammation and oxidative stress. *Oxidative Medicine and Cellular Longevity*, 2019, 9659757. <https://doi.org/10.1155/2019/9659757>
 72. Zhang, H., Neuhöfer, P., Song, L., Rabe, B., Lesina, M., Kurkowski, M.U., Treiber, M., Wartmann, T., Regné, S., Thorlacius, H., Saur, D., Weirich, G., Yoshimura, A., Halangk, W., Mizgerd, J.P., Schmid, R.M., Rose-John, S., Algül, H., 2013. IL-6 trans-signaling promotes pancreatitis-associated lung injury and lethality. *The Journal of Clinical Investigation*, 123, 1019-1031. <https://doi.org/10.1172/JCI64931>